Crystal structure of a phleboviral Gc glycoprotein reveals a consolidated model of membrane fusion

Steinar Halldorsson[1], Anna-Janina Behrens[2], Karl Harlos[1], Juha T. Huiskonen[1], Richard M. Elliott[3], Max Crispin[2], Benjamin Brennan[3]*, Thomas A. Bowden*[1]

[1]Division of Structural Biology, Wellcome Trust Centre for Human Genetics, University of Oxford, Roosevelt Drive, Oxford OX3 7BN, United Kingdom. [2]Oxford Glycobiology Institute, Department of Biochemistry, University of Oxford, South Parks Road, Oxford OX1 3QU, United Kingdom. [3]MRC-University of Glasgow Centre for Virus Research, Institute of Infection, Immunity and Inflammation, College of Medical, Veterinary and Life Sciences, University of Glasgow, 464 Bearsden Road, Glasgow G61 1QH, United Kingdom.

Submitted to Proceedings of the National Academy of Sciences of the United States of America

An emergent viral pathogen termed 'severe fever with thrombocytopenia syndrome virus' (SFTSV) is responsible for thousands of clinical cases and associated fatalities in China, Japan, and South Korea. Akin to other phleboviruses, SFTSV relies on a viral glycoprotein, Gc, to catalyze the merger of endosomal host and viral membranes during cell entry. Here, we describe the trimeric postfusion structure of SFTSV Gc, revealing that the molecular transformations the phleboviral Gc undergoes upon host cell entry are conserved with otherwise unrelated alpha- and flaviviruses. By comparison of SFTSV Gc with that of the prefusion structure of the related Rift Valley fever virus, we show that these changes involve a dimer-to-trimer transition and refolding of the protein. Reverse genetics and rescue of site-directed histidine mutants enabled localization of histidines likely to be important for triggering this pH-dependent process. These data provide structural and functional evidence that the mechanism of phlebovirus–host cell fusion is conserved among genetically and patho-physiologically distinct viral pathogens.

Emerging virus | Phlebovirus | Viral membrane fusion | Glycoprotein | Structure

Introduction

Severe fever with thrombocytopenia syndrome virus (SFTSV, also known as Huaiyangshan virus) constitutes one of the most dangerous human pathogens within the *Phlebovirus* genus of the *Bunyaviridae* family. Since emerging in China in 2009, thousands of infections have been reported in humans throughout China, South Korea, and Japan. Upon zoonosis from ticks to humans, SFTSV causes thrombocytopenia, leukocytopenia, febrile illness and, in severe cases, encephalitis (1-3). SFTSV belongs to the Bhanja phlebovirus serocomplex and genomic analysis reveals that the virus has evolved extensively over the last 150 years, having diverged into at least five different clusters (4). Although a recent study suggested that many SFTSV infections are subclinical (5), mortality rates reach up to 30% in a clinical setting (1) and there are currently no vaccines or antivirals against the virus.

The negative-sense and single-stranded genome of SFTSV is divided into three RNA segments, S, M, and L. The M segment encodes two glycoproteins, Gn and Gc, which facilitate host cell entry and are derived by cleavage of a polyprotein precursor by cellular proteases during translation (6). Similar to related phleboviruses, Rift Valley fever virus (RVFV) and Uukuniemi virus (UUKV), SFTSV Gn and Gc likely form higher order pentamers and hexamers on the virion envelope in an icosahedral $T = 12$ symmetry (7-10). The N-linked glycans displayed by this glycoprotein complex are important determinants of tissue and receptor tropism and are recognized by the C-type lectin host cell receptor, DC-SIGN, during viral attachment (11, 12). Following receptor recognition, the virion is endocytosed into the host cell (13-15) and the metastable Gc orchestrates fusion of endosomal and viral membranes, facilitating release of viral RNA into the cytosol. Interestingly, SFTSV is also capable of cell entry via extracellular vesicles, which likely allows evasion of the host immune system (16). Structural studies of the cognate Gc from RVFV (17) in the prefusion conformation revealed that the phleboviral Gc forms a class II architecture, which has been also observed for envelope glycoproteins from positive-sense RNA viruses from the *Togaviridae* and *Flaviridae* families (18, 19). A similar class II architecture has also been observed in cell-cell fusion proteins, although the mechanism of membrane fusion is likely to differ from viral fusion as evident by the absence of a hydrophobic fusion loop (20).

A detailed mechanism of membrane fusion by class II viral fusion proteins has been proposed, where pH-dependent triggering of the glycoprotein is thought to arise during endosomal trafficking of the virus (21-23). It is expected that the acidic environment within endocytotic compartments activates a 'histidine-switch', which disrupts protein-protein contacts on the virion surface such that a hydrophobic fusion peptide located at the apex of the molecule is exposed and extended into the target host membrane. Upon membrane binding, togaviral and flaviviral fusion glycoproteins form trimers (21, 24) which are believed to trigger hemifusion (25, 26). The concerted action of two or more trimers is thought to be required to draw together virion and host cell membranes, in a process ultimately leading to membrane merger (25, 26).

To deepen our understanding of the mechanism of phlebovirus-–host cell membrane fusion during host cell infection, we solved the crystal structure of the soluble ectodomain of SFTSV Gc to 2.45-Å resolution. SFTSV Gc

Significance

'Severe fever with thrombocytopenia syndrome virus' (SFTSV) is a deadly tick-borne viral pathogen. Since first being reported in China, 2009, SFTSV has spread throughout South Korea and Japan, with mortality rates reaching up to thirty percent. The surface of the SFTSV virion is decorated by two glycoproteins, Gn and Gc. Here, we report the atomic-level structure of the Gc glycoprotein in a conformation formed during uptake of the virion into the host cell. Our analysis reveals the conformational changes that the Gc undergoes during host cell infection and provides structural evidence that these rearrangements are conserved with otherwise unrelated alpha- and flaviviruses.

Reserved for Publication Footnotes

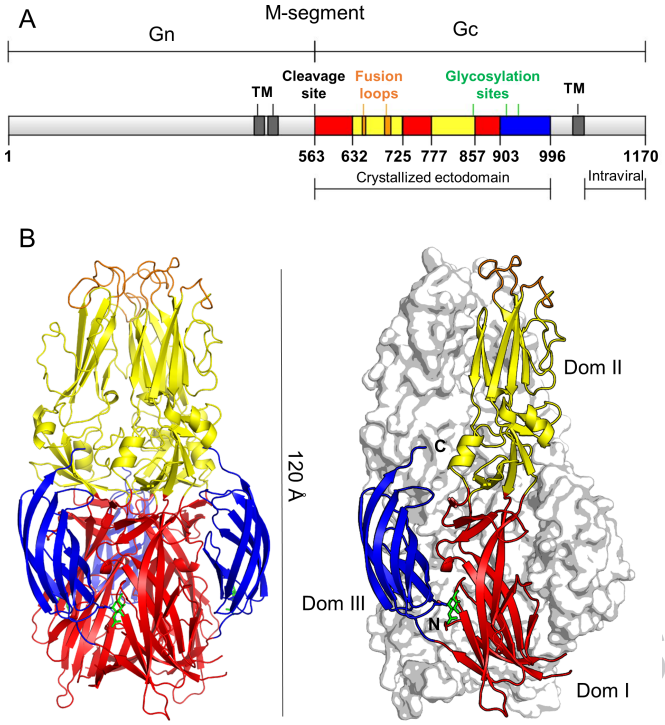

Fig. 1. Crystal structure of SFTSV Gc in the postfusion conformation. **A)** Domain diagram of the full M-segment of SFTSV containing Gn and Gc with the crystallized ectodomain colored by domain: domain I in red, domain II in yellow, and domain III in blue. **B)** SFTSV Gc in the postfusion trimeric conformation. The full trimer is shown on the left side in cartoon representation and is colored according to domain as in panel A. Glycans observed in the crystal structure are shown as green sticks. On the right side, a single protomer is shown in cartoon representation with the remainder of the trimer shown as a white van der Waals surface.

crystallized in a three domain (I–III), trimeric postfusion configuration. By comparison of our SFTSV Gc structure to the prefusion structure of the RVFV Gc, we show that the fusogenic rearrangements of the phleboviral Gc are analogous to those observed for the envelope fusion glycoproteins of alpha- (family *Togaviridae*) and flaviviruses (family *Flaviviridae*), indicating a conserved mechanism of membrane fusion between these otherwise non-related groups of viruses. Interestingly, we identify two putative fusion loops, which are likely inserted into the host membrane during host cell entry. The conformation of these hydrophobic loops remains unchanged between pre- and postfusion RVFV and SFTSV Gc structures despite exhibiting low sequence conservation. By reverse genetics and rescue of site-directed fusion loop mutants, we show that these residues are stringently required for the virus lifecycle. We also present evidence that histidines in domains I and III of the Gc are essential for the virus life cycle and, by analogy to RVFV (15), likely contribute to the pH-induced conformational rearrangements of the molecule. These data provided structural and functional evidence for a unified mechanism of membrane fusion between phlebo-, flavi-, and alphaviruses.

Results and Discussion

The SFTSV Gc ectodomain forms putative trimers at acid pH. The ectodomain of SFTSV Gc (residues 563–996, **Fig. 1A**), lacking 39 residues proximal to the predicted C-terminal transmembrane region, was recombinantly expressed in human embryonic kidney (HEK) 293T cells in the presence of the α-mannosidase I inhibitor, kifunensine (27). Soluble SFTSV Gc was purified from cell supernatant and N-linked glycosylation was cleaved to single acetylglucosamine (GlcNAc) moieties with endoglycosidase F_1 (28).

Table 1. Crystallographic data collection and refinement

Data collection	K_2PtCl_6 SAD data	Native data
Beamline	I04, DLS	I03, DLS
Resolution range (Å)	108.62-2.89 (2.97-2.89)	108.51-2.45 (2.51-2.45)
Space group	$I2_12_12_1$	$I2_12_12_1$
Cell dimensions		
a, *b*, *c* (Å)	147.2, 152.3, 160.9	147.4, 152.3, 160.4,
α, β, γ (°)	90.0, 90.0, 90.0	90.0, 90.0, 90.0
No. of crystals	3	2
Wavelength (Å)	1.072	1.008
Unique reflections	40,765 (2,964)	66,293 (4,838)
Completeness (%)	99.9 (98.9)	99.8 (99.3)
R_{merge} (%)[a]	16.4 (63.7)	10.2 (108.4)
I/σI	22.1 (2.6)	15.7 (1.8)
Avg. redundancy	34.1 (6.0)	8.1 (7.8)
Refinement		
Resolution range		108.51-2.45 (2.51-2.45)
Number of reflections		66,125 (2,792)
R_{work} (%)[b]		19.0
R_{free} (%)[c]		23.2
RMSD		
Bonds (Å)		0.002
Angles (°)		0.500
Molecules per a.s.u.		3
Atoms per a.s.u (protein/carbohydrate/ water)		9,565/42/104
Average *B*-factors (Å^2) (protein/carbohydrate/ water)		81.3/103.6/62.5
Ramachandran plot (%)		
Most favoured region		96.9
Allowed region		3.0
Outliers		0.1

Numbers in parentheses refer to the relevant outer resolution shell. r.m.s.d.: root mean square deviation from ideal geometry.
[a] $R_{merge} = \Sigma_{hkl}\ \Sigma_i|I(hkl;i) - \langle I(hkl)\rangle|/\Sigma_{hkl}\ \Sigma_i I(hkl;i)$, where $I(hkl;i)$ is the intensity of an individual measurement and $\langle I(hkl)\rangle$ is the average intensity from multiple observations.
[b] $R_{factor} = \Sigma_{hkl}||F_{obs}| - k|F_{calc}||/\Sigma_{hkl}\ |F_{obs}|$
[c] R_{free} equals the *R*−factor as calculated above but using against 5% of the data removed prior to refinement.

Similar to that observed for the Gc glycoprotein from the related RVFV Gc (17), SFTSV Gc eluted as a single monomeric species on size exclusion at neutral pH (8.0). Upon acidification (5.0), we observed a mixture of monomeric and putative trimeric species, consistent with rearrangements of the molecule to a post-fusion state (**Fig. S1**) (29). These observations are suggestive that an acidic environment is necessary for the formation of SFTSV Gc trimers.

Crystal structure of SFTSV Gc in the trimeric postfusion conformation. The structure of SFTSV Gc was solved by the single wavelength anomalous diffraction method (SAD), with a platinum derivative (K_2PtCl_6) (**Table 1**). A single trimer of SFTSV Gc was observed in the asymmetric unit. In line with both our size exclusion analysis at acidic pH (**Fig. S1**) and previously reported structures of dengue virus (DENV) E (21) and Semliki Forest virus (SFV) E1 (24) glycoproteins in trimeric states, we suggest that our SFTSV Gc is in a postfusion conformation. Each protomer of the trimer is composed of three domains: I,

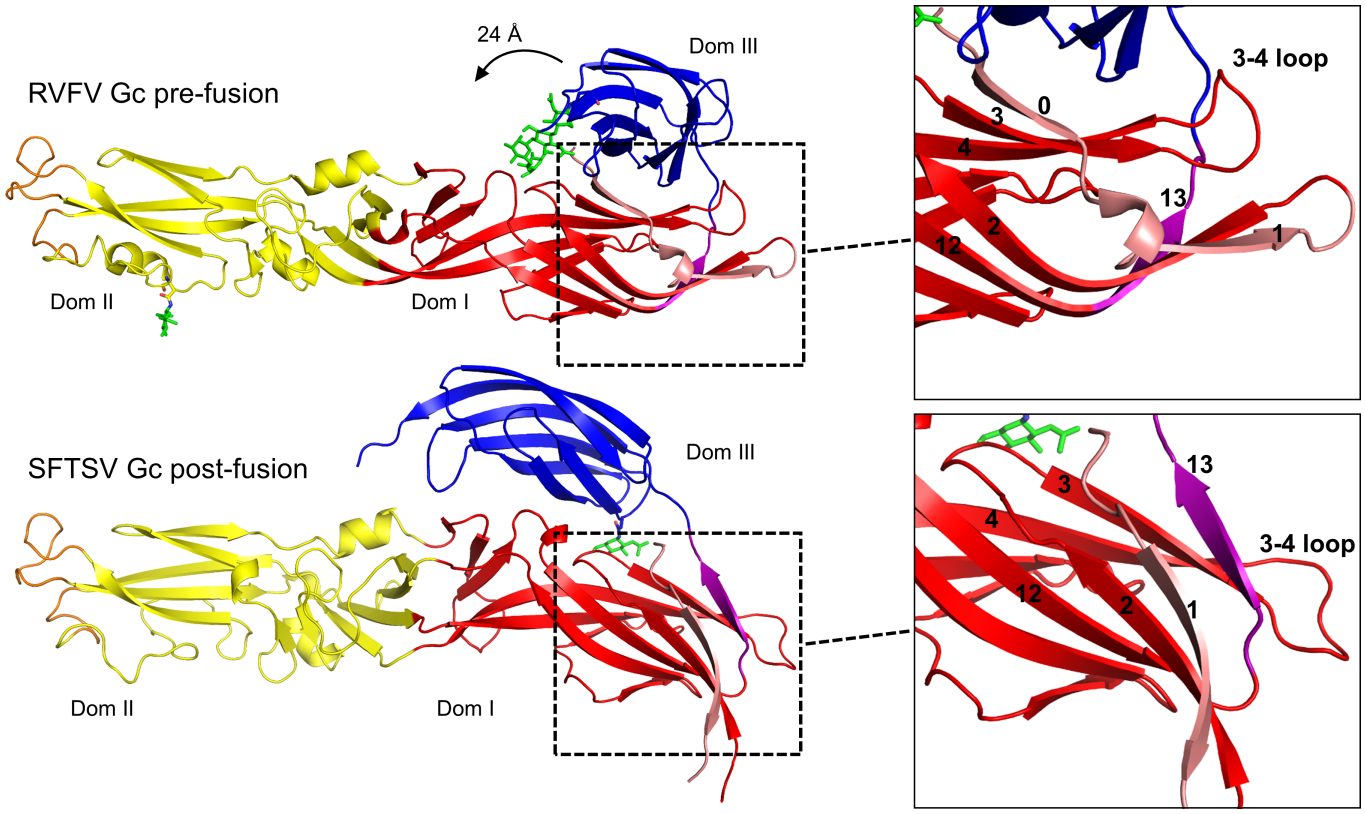

Fig. 2. Structural rearrangements of phleboviral Gc from prefusion to postfusion conformations. Single protomers of RVFV Gc (PDB accession no. 4HJ1) and SFTSV Gc are shown in cartoon representation and colored as in Fig. 1. Glycans are shown as green sticks. Zoom-in panels of domain I are shown on the right side and highlight the strand swap occurring between pre- and postfusion states. In the postfusion conformation, strand no. 13 (purple) reorientates around the 3-4 loop, forming a β-sheet with strands no. 3 and 4, and strand no. 0 (pink) becomes continuous with strand no. 1 (pink).

II, and III (**Fig 1B**). Domain I consists of an elongated thirteen-stranded β-sandwich at the central core of the structure, domain II consists of a five-stranded β-sandwich and a six-stranded β-sheet, and domain III consists of a seven-stranded β-barrel-like module and forms extensive protein-protein contacts (1,321 Å^2) with domain I. Overlay analysis reveals little deviation in structure between symmetry-related Gc protomers. The average root-mean-square-deviation (RMSD) was 0.64 Å over 428 Cα residues, with the greatest differences detected at regions responsible for forming crystallographic contacts (**Fig. S2**). Unlike what has been observed SFV E1 (24), analysis of crystallographic packing did not reveal any physiologically relevant higher order oligomeric arrangements of SFTSV Gc trimers.

The SFTSV Gc ectodomain is stabilized by thirteen disulphide bonds in a pattern that is well-conserved across phleboviruses (**Fig. S3**). In addition to these disulphide bond pairs, we also observed an unpaired cysteine, Cys617, in domain I of the molecule. Cys617 is solvent exposed and located in close proximity to the Cys563−Cys604 disulphide pairing (**Fig. S4**). This lone cysteine is present in Heartland phlebovirus Gc but a phenylalanine (Phe744) is found in the equivalent position in RVFV Gc (**Fig. S4**). Mutagenesis of the cysteine to methionine (C617M) had no effect upon soluble expression of SFTSV Gc (**Fig. S5**). Similarly, rescue of live SFTSV further confirmed that this aberrant cysteine has little influence upon virus replication, where the C617M mutant recovered to wild-type levels (**Fig. S4**).

We note that in addition to this free cysteine being present in several species of SFTSV, it is also observed in the related Heartland phlebovirus (**Fig. S3**). Indeed, unpaired cysteines, with no obvious functional roles, have also been observed in other virus families. For example, such a free cysteine motif has been observed on the attachment glycoprotein of an African henipavirus (30).

Rearrangements of Gc are conserved with flavi- and alphaviruses. The crystal structure of RVFV Gc in the prefusion conformation constitutes the closest structural relative of SFTSV Gc (~25% sequence identity) (17). Structural comparison of prefusion RVFV Gc and postfusion SFTSV Gc revealed that the transition from pre- to postfusion states involves major conformational changes to the molecule (**Fig. 2**). While the pre- and postfusion conformations of the primarily β-stranded domain III (RMSD of 1.16 Å over 81 Cα residues) are very similar (**Fig. S6A**), large structural rearrangements are observed upon overlay of domain II (RMSD of 2.13 Å over 117 Cα residues, **Fig. S6B**) and domain I (3.41-Å RMSD over 109 Cα residues, **Fig. S6C**) of RVFV Gc and SFTSV Gc. Structural changes to domain I include modifications to secondary structure, where hydrogen bonds linking the first strand, '0', of the β-sandwich to the third strand, '3', are displaced and replaced by an extension of the last β-strand, '13' (**Fig. 2**). A similar restructuring also occurs in the fusogenic rearrangements of SFV E1 protein (24, 31) and DENV E protein (21).

In addition to domain I refolding, we also observed a 24-Å shift in the position of domain III between pre- (RVFV Gc) and postfusion (SFTSV Gc) conformations (**Fig. 2**). In our postfusion SFTSV Gc structure, the amount of protein−protein contacts made by a single domain III with the rest of the oligomeric assembly is more than two times greater (1,321 Å^2) than that observed for domain III in the prefusion RVFV Gc structure (570 Å^2) (32). Similarly, an increase in protein-protein contacts made by domain III has been observed in DENV E (21, 33) (from 826

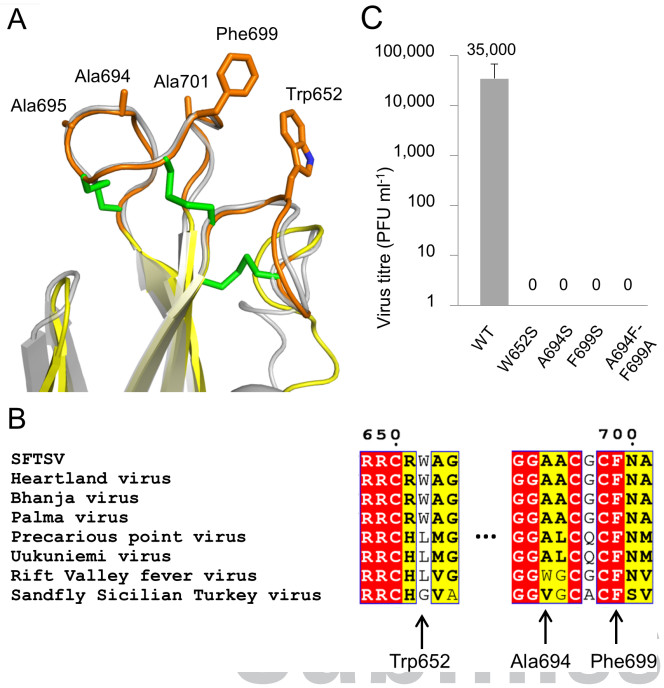

Fig. 3. The putative fusion loops of SFTSV Gc are conformationally rigid and contain essential residues. **A)** An overlay of the fusion loops of SFTSV Gc (colored as in Fig. 1) and RVFV Gc (gray, PDB accession no. 4HJ1) reveals highly similar conformations. Side chains from hydrophobic amino acids from SFTSV Gc are shown as orange sticks. Disulphide bonds are shown as green sticks. **B)** Sequence alignment of fusion loops across selected phleboviruses. Residues highlighted red are fully conserved and yellow are partially conserved. Residues tested by site-directed mutagenesis are highlighted by arrows. Phe699 is fully conserved while Trp652 is more varied amongst phleboviral sequences. **C)** SFTSV encoding single and double site-directed mutations at the putative fusion loops were derived by reverse genetics and the titers of these recombinant viruses, measured in plaque forming units (PFU), were compared with wild type (WT) SFTSV.

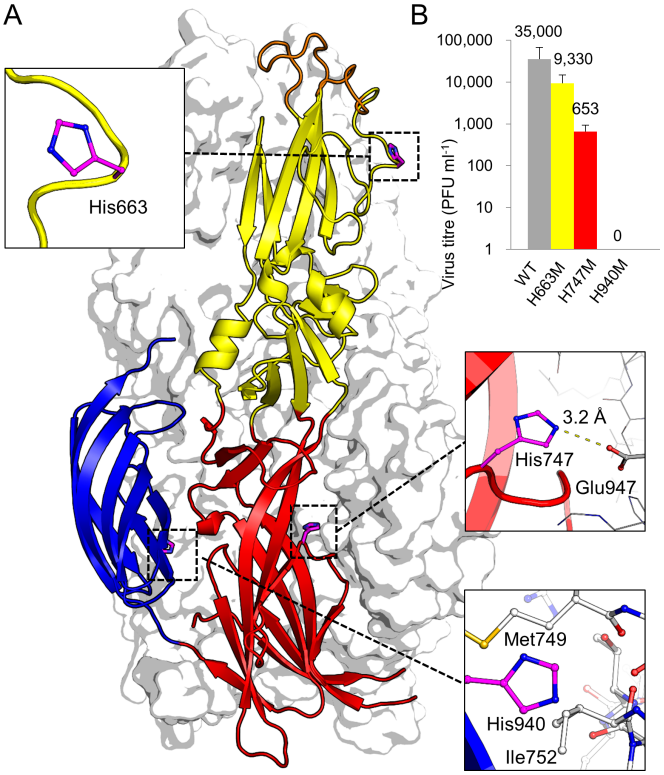

Fig. 4. Surface exposed His663, His747 and His940 on on SFTSV Gc domains I and III play integral roles in the virus life cycle. **A)** A singleSFTSV Gc protomer is shown in cartoon representation (colored as in Fig. 1) with the remainder of the trimer shown as a white van der Waals surface. Surface exposed histidines are shown as purple sticks. Zoom-in panels highlight the location of these residues within each of the three domains and residues surrounding His747 and His940 from adjacent protomers are shown as white sticks **B)** SFTSV encoding single mutations of His663, His747 and His940 were derived by reverse genetics and the titers of these recombinant viruses, measured in PFU, were compared with that of WT SFTSV.

to 1,315 Å^2) and SFV E1 (24, 31) proteins (from 572 to 1,530 Å^2). It is likely that the formation of such extended protein–protein contacts is energetically favorable and stabilize the postfusion conformation of the Gc (24).

The conformationally conserved hydrophobic fusion loops. An essential feature of the class-II fusion glycoprotein architecture is the hydrophobic fusion loop located at the apex of domain II, which is inserted into the host membrane and draws the viral and host membranes together upon fusogenic rearrangements of the molecule (34). In contrast to a single fusion loop, which performs this function in alpha- and flaviviruses, structural analysis of RVFV Gc in the prefusion state revealed two putative fusion loops. These loops are also present in SFTSV Gc (Cys650–Cys656, loop 1; Cys691–Cys705, loop 2) and are similarly composed of hydrophobic amino acids, including Ala694, Ala695, Ala701, Trp652, and Phe699 (**Fig. 3A**). However, in contrast to the prefusion RVFV Gc structure, these loops are fully solvent accessible and not concealed within oligomeric protein–protein contacts. Interestingly, these loops form a strikingly similar conformation to that observed in RVFV Gc (17), where superposition reveals little difference in structure (RMSD of 0.75 Å over 22 Cα residues) (**Fig. 3A**). The conserved conformation of the two loops is consistent with that observed in the DENV E protein fusion loop (21), but contrasts the conformational changes observed in the fusion loop of SFV E1 protein (24), which may occur as a result of crystallographic packing.

Aromatic residues Trp652 and Phe699, from loops 1 and 2, respectively, dominate the hydrophobic landscape of these putative fusion loops and extend outwards towards the solvent. Given the relative size and positioning of the Trp652 and Phe699 sidechains away from the molecule and toward a hypothetical virion membrane surface, we hypothesized that these residues must be functionally indispensable for virus infectivity. To assess the importance of these residues, we performed rescue of live SFTSV with single mutations W652S, A694S, and F699S, and a double mutant, A694F/F699A (**Fig. 3C**). Whilst these mutants still passed through the folding pathway required for secretion (**Fig. S5**), they proved refractory to replication in the context of live virus. These results underscore the sensitivity of this loop region to sequence variation (**Fig. 3B**), whereby only limited changes in sequence can preserve functionality.

N-linked glycosylation on SFTSV Gc. Three N-linked glycosylation sequons are present in our expressed SFTSV Gc ectodomain: As853, Asn914, and Asn936. Analysis of electron density at these sites in each of the three protomers revealed the presence of N-acetylglucosamine (GlcNAc) moieties at Asn914 and at least partial occupancy at Asn936. No glycan electron density was observed at Asn853, but as with Asn936, this may arise due to linkage flexibility as well as incomplete sequon occupancy (**Fig. S7**).

Given that SFTSV entry into a host cell is DC-SIGN-dependent (12) and that the glycans presented by the related UUKV Gc are predominantly oligomannose-type (35-37), it is likely that Gc glycosylation on SFTSV is important for lectin-mediated host cell entry. To assess whether the Gc glycans are accessible to processing during recombinant expression, we per-

formed glycan analysis by HILIC-UPLC (hydrophilic interaction chromatography-ultra performance liquid chromatography) and assessed the levels of oligomannose-type glycans using endoglycosidase H digestion (**Fig. S8**). Unlike our glycoprotein preparations for crystallography, no mannosidase inhibitors were included during expression. We observed negligible levels of hybrid- and oligomannose-type populations with the spectrum dominated with processed complex-type glycans. This suggests a model whereby any oligomannose-type glycans that may contribute to DC-SIGN-mediated attachment are likely to arise only through steric limitations to glycan processing due to the higher order protection effects by the quaternary Gn-Gc assembly. We note that across the phleboviral genus the number and position of glycosylation sites are not well conserved, suggesting that the DC-SIGN dependency for infection may be variable (**Fig. S9**) and that the presentation of putative DC-SIGN glycan ligands is likely to be heterogeneous.

Histidine-dependent function. Surface exposed histidine residues are a canonical feature of class-II fusion machinery (38, 39). During virion trafficking through endosomal compartments, protonation of histidine-imidazole side-chains (at pK_a ~6.0) is thought to trigger conformational changes of the fusion protein, catalyzing merger of virion and host membranes (15, 40). Such residues are often found in charged environments and may form irreversible salt bridges or hydrogen bonds with negatively charged residues, stabilizing the postfusion conformation of the glycoprotein (39). In alpha- and flaviviruses, many of these functionally important histidines appear to co-localize near the interface between domains I and III (41, 42).

A similar histidine dependency has been observed for phleboviruses, with Gc residues His778, His857, and His1087 having been shown to be key for RVFV infectivity (15). However, in contrast to the localized patch of functionally important histidines in alpha- and flaviviruses, His778, His857, and His1087 are interspersed throughout domains I, II, and III of RVFV Gc, respectively. While no functional role for His857 was suggested by crystallographic analysis of RVFV Gc, His778 has been proposed to stabilize Gc fusion peptide-host envelope interactions and His1087 co-localizes near the domain I/III interface (17). Interestingly, none of these histidines are conserved with SFTSV Gc. Nevertheless, we were able to identify histidines, His663, His747, and His940, at nearby sites on our SFTSV Gc structure (**Fig. 4A**). To assess the functional importance of these residues, we introduced single H663M, H747M, and H940M mutations to SFTSV Gc. While none of these mutations had an observable effect upon protein folding or secretion of soluble SFTSV Gc (**Fig. S5**), only the H663M mutation could be rescued to levels close to the wild-type using our reverse genetics system. Indeed, H747M was rescued to very low titers and H940M could not be rescued (**Fig. 4B**). The sensitivity of the SFTSV lifecycle to these mutations is consistent with the histidine-triggered fusion mechanism observed in alpha- and flaviviruses (41, 43). Additionally, as observed in DENV E, where histidine residues stabilize the post-fusion conformation of the glycoprotein (42), H747 forms a hydrogen bond that may stabilize the postfusion conformation of SFTSV Gc (**Fig. 4A**). The successful rescue of H663M, on the other hand, is suggestive this residue is not as crucial for virus replication and may not play a substantial role in stabilizing the fusion peptide-host envelope interaction, as suggested for His778 in RVFV (17). These data highlight the importance of surface-exposed histidines in the phleboviral lifecycle and reveal that these residues need not be absolutely conserved amongst phleboviruses to play similar functional roles.

Conclusions

It is now evident that the phleboviral Gc fusion glycoprotein is both functionally and structurally analogous to the fusion glycoproteins of alpha- and flaviviruses. Similarly, our analyses revealed that the phleboviral Gc adopts a trimeric postfusion arrangement, encodes fusion loops at the apex of the molecule, and is functionally dependent upon surface exposed histidines for virus replication. In addition to this conserved functionality, alpha-, flavi-, and phleboviruses are also united in their ability to recognize DC-SIGN receptor to enable viral attachment (44, 45), a recognition event facilitated by the presentation of oligomannose-type carbohydrates on the viral surface. These biosynthetically immature glycans are generally an uncommon feature amongst secreted cellular glycoproteins and our data suggests that such carbohydrate structures arise from constraints on glycan biosynthesis imposed by the local virus structure during folding and assembly. Indeed, the influence of local protein structure in limiting glycan processing has been observed in many viruses, including alpha- (46) and flaviviruses (47).

It is interesting to contemplate the evolutionary origin of this conserved class-II fold, especially as this architecture has been observed in cell-cell fusion proteins (20). Given the absence of any apparent genetic homology between organisms utilizing this fold for membrane fusion, it is conceivable that the class-II fusion scaffold has evolved considerably from a common viral ancestor, as has been suggested for the lineage of viruses harbouring upright β-barrel capsid proteins (48). Alternatively, as revealed by the crystal structure of the *Caenorhabditis elegans* EFF-1 fusion protein (20), it possible that the class-II fold is of cellular origin and viruses have added additional functionality to the scaffold (e.g. the addition of hydrophobic fusion peptide(s)) after independently 'borrowing' it in the process. Irrespective, the conservation of this fold is reflective of the absolute necessity for genetically and patho-biologically diverse viruses to preserve a fundamental function throughout a long evolutionary history.

Materials and methods

Protein expression and purification. The ectodomain of SFTSV Gc, residues 563–996 from M-segment (UniProt accession no. R4V2Q5), was cloned into the pHLSec vector (49). HEK293T cells were transiently transfected with 2 mg of DNA per litre of cell media in the presence of 1 μg/ml kifunensine (28). The supernatant was collected 5 to 6 days after transfection, clarified and dialyzed against buffer containing 10 mM Tris-HCl pH 8.0 and 150 mM NaCl. The dialysed protein was captured by immobilized metal affinity chromatography using a HisTrap nickel column and deglycosylated overnight at room temperature using endoglycosidase F_1 (67 μg per 1 mg of protein). Deglycosylated Gc was further purified by size exclusion chromatography using a Superdex 200 10/30 column in buffer containing 10 mM Tris-HCl pH 8.0 and 150 mM NaCl. The total yield of purified and deglycosylated SFTSV Gc was approximately 0.5 mg per litre of tissue culture media.

Crystallization and structure determination. SFTSV Gc ectodomain was crystallized using the sitting-drop vapour method (50) after five days with a protein concentration of 3.5 mg/ml in precipitant containing 45% pentaerythriotol 426, 0.1 M sodium acetate at pH 4.6 (51). Crystals were cryo-cooled in precipitant solution using liquid nitrogen. Native X-ray data was collected at 1.00862-Å wave-length on a PILATUS 6M detector at Diamond Light Source (DLS) on beamline I03. X-ray data were indexed, integrated and scaled in XIA2 (52). Crystallographic statistics are summarized in Table 1. For phasing, crystals were soaked in K_2PtCl_6 for ninety minutes. Peak anomalous data was collected at the LIII edge of platinum on a PILATUS 6M detector at DLS on beamline I04 at 1.07206 Å. Initial phases were obtained using the SAD method in autoSHARP (53) and Buccaneer, as implemented in autoSHARP, was used for initial model building (54). The first rounds of refinement were carried out using Refmac5 (55) and then PHENIX (56) with TLS restraints. Manual model building was performed in Coot (57) and final structure validation was done using MolProbity (58).

Generation of recombinant SFTSV from cDNA. Plasmid pTVT7-HB29M containing a full-length cDNA to the HB29 M segment (GenBank accession number KP202164) was mutated by site directed mutagenesis to introduce the following single amino acid substitutions (W652S, A694S, F699A, C563M, C604M, C617M, H663M, H747M, H940M) and double amino acid substitution (A694F-F699A) into the HB29 M polyprotein. Recombinant SFTSV were generated as previously described (59). Three independent attempts were performed for each Gc mutant with corresponding wild-type controls. After 5 days, the virus-containing supernatants were collected, clarified by low speed centrifugation and stored at -80 °C. Stocks of recombinant viruses were grown in Vero E6 cells at 37°C by infecting at multiplicity of infection of 0.01 and harvesting the culture medium at 7 days postinfection.

Virus titration by plaque assay. Vero E6 cells were infected with serial dilutions of virus and incubated under an overlay consisting of DMEM supplemented with 2% FCS and 0.6% Avicel (FMC BioPolymer) at 37°C for 7 days. Cell monolayers were fixed with 4% formaldehyde. Following fixation, cell monolayers were stained with Giemsa to visualize plaques.

Data Deposition. Atomic coordinates and structure factors of SFTSV Gc have been deposited in the PDB (accession code 5G47).

ACKNOWLEDGEMENTS.

We thank the staff of beamlines I03 and I04 at DLS for support. K.H. is supported by the Medical Research Council (MRC, grant MR/N00065X/1) and J.H. by the European Research Council under the European Union's Horizon 2020 research and innovation programme (649053). Work in the laboratory of M.C. is supported by the International AIDS Vaccine Initiative Neutralizing Antibody Center CAVD grant and the Scripps CHAVI-ID (1UM1AI100663). Work at the University of Glasgow is supported by a Wellcome Trust Senior Investigator award to R.M.E. (No. 099220/Z/12/Z). T.A.B. is supported by the MRC (MR/L009528/1 and MR/N002091/1). The Wellcome Trust Centre of Human Genetics is funded through a Core Award (090532/Z/09/Z).

1. Yu X-J, *et al.* (2011) Fever with thrombocytopenia associated with a novel bunyavirus in China. *The New England journal of medicine* 364:1523-1532.
2. Cui N, *et al.* (2014) Severe fever with thrombocytopenia syndrome bunyavirus-related human encephalitis. *The Journal of infection*.
3. Ding F, *et al.* (2013) Epidemiologic features of severe fever with thrombocytopenia syndrome in China, 2011-2012. *Clinical infectious diseases : an official publication of the Infectious Diseases Society of America* 56:1682-1683.
4. Lam TT-Y, *et al.* (2013) Evolutionary and molecular analysis of the emergent severe fever with thrombocytopenia syndrome virus. *Epidemics* 5:1-10.
5. Zhang L, *et al.* (2014) Antibodies against Severe Fever with Thrombocytopenia Syndrome Virus in Healthy Persons, China, 2013. *Emerging infectious diseases* 20:1355-1357.
6. Ulmanen I, Seppala P, & Pettersson RF (1981) In vitro translation of Uukuniemi virus-specific RNAs: identification of a nonstructural protein and a precursor to the membrane glycoproteins. *J. Virol.* 37(1):72-79.
7. Freiberg AN, Sherman MB, Morais MC, Holbrook MR, & Watowich SJ (2008) Three-dimensional organization of Rift Valley fever virus revealed by cryoelectron tomography. *J. Virol.* 82(21):10341-13048.
8. Huiskonen JT, Överby AK, Weber F, & Grünewald K (2009) Electron cryo-microscopy and single-particle averaging of Rift Valley fever virus: evidence for GN-GC glycoprotein heterodimers. *J. Virol.* 83(8):3762-3769.
9. Overby AK, Pettersson RF, Grünewald K, & Huiskonen JT (2008) Insights into bunyavirus architecture from electron cryotomography of Uukuniemi virus. *Proc. Nat. Acad. Sci. USA* 105(7):2375-2379.
10. Sherman MB, Freiberg AN, Holbrook MR, & Watowich SJ (2009) Single-particle cryo-electron microscopy of Rift Valley fever virus. *Virology* 387(1):11-15.
11. Lozach PY, *et al.* (2011) DC-SIGN as a receptor for phleboviruses. *Cell Host Micr.* 10(1):75-88.
12. Hofmann H, *et al.* (2013) Severe fever with thrombocytopenia virus glycoproteins are targeted by neutralizing antibodies and can use DC-SIGN as a receptor for pH-dependent entry into human and animal cell lines. *J. Virol.* 87(8):4384-4394.
13. Harmon B, *et al.* (2012) Rift Valley fever virus strain MP-12 enters mammalian host cells via caveola-mediated endocytosis. *J. Virol.* 86(23):12954-12970.
14. Lozach PY, *et al.* (2010) Entry of bunyaviruses into mammalian cells. *Cell host & microbe* 7(6):488-499.
15. de Boer SM, *et al.* (2012) Acid-activated structural reorganization of the Rift Valley fever virus Gc fusion protein. *Journal of virology* 86(24):13642-13652.
16. Silvas JA, Popov VL, Paulucci-Holthauzen A, & Aguilar PV (2015) Extracellular Vesicles Mediate Receptor-Independent Transmission of Novel Tick-Borne Bunyavirus. *Journal of virology* 90(2):873-886.
17. Dessau M & Modis Y (2013) Crystal structure of glycoprotein C from Rift Valley fever virus. *Proceedings of the National Academy of Sciences of the United States of America* 110:1696-1701.
18. Rey FA, Heinz FX, Mandl C, Kunz C, & Harrison SC (1995) The envelope glycoprotein from tick-borne encephalitis virus at 2 A resolution. *Nature* 375(6529):291-298.
19. Lescar J, *et al.* (2001) The Fusion glycoprotein shell of Semliki Forest virus: an icosahedral assembly primed for fusogenic activation at endosomal pH. *Cell* 105(1):137-148.
20. Perez-Vargas J, *et al.* (2014) Structural basis of eukaryotic cell-cell fusion. *Cell* 157(2):407-419.
21. Modis Y, Ogata S, Clements D, & Harrison SC (2004) Structure of the dengue virus envelope protein after membrane fusion. *Nature* 427:313-319.
22. Stiasny K, Allison SL, Marchler-Bauer A, Kunz C, & Heinz FX (1996) Structural requirements for low-pH-induced rearrangements in the envelope glycoprotein of tick-borne encephalitis virus. *Journal of virology* 70:8142-8147.
23. Bitto D, Halldorsson S, Caputo A, & Huiskonen JT (2016) Low pH and Anionic Lipid Dependent Fusion of Uukuniemi Phlebovirus to Liposomes.
24. Gibbons DL, *et al.* (2004) Conformational change and protein-protein interactions of the fusion protein of Semliki Forest virus. *Nature* 427(6972):320-325.
25. Chao LH, Klein DE, Schmidt AG, Pena JM, & Harrison SC (2014) Sequential conformational rearrangements in flavivirus membrane fusion. *eLife* 3:e04389.
26. Esposito DL, Nguyen JB, DeWitt DC, Rhoades E, & Modis Y (2015) Physicochemical requirements and kinetics of membrane fusion of flavivirus-like particles. *The Journal of general virology*.
27. Elbein AD, Tropea JE, Mitchell M, & Kaushal GP (1990) Kifunensine, a potent inhibitor of the glycoprotein processing mannosidase I. *JBC* 265(26):15599-15605.
28. Chang VT, *et al.* (2007) Glycoprotein Structural Genomics: Solving the Glycosylation Problem. *Structure* 15(3):267-273.
29. Vaney MC & Rey FA (2011) Class II enveloped viruses. *Cell. Microbiol.* 13(10):1451-1459.
30. Lee B, *et al.* (2015) Molecular recognition of human ephrinB2 cell surface receptor by an emergent African henipavirus. *Proc Natl Acad Sci U S A* 112(17):E2156-2165.
31. Roussel A, *et al.* (2006) Structure and interactions at the viral surface of the envelope protein E1 of Semliki Forest virus. *Structure (London, England : 1993)* 14:75-86.
32. Krissinel E & Henrick K (2007) Inference of macromolecular assemblies from crystalline state. *J. Mol. Biol.* 372(3):774-797.
33. Modis Y, Ogata S, Clements D, & Harrison SC (2003) A ligand-binding pocket in the dengue virus envelope glycoprotein. *Proceedings of the National Academy of Sciences of the United States of America* 100:6986-6991.
34. Modis Y, Ogata S, Clements D, & Harrison SC (2004) Structure of the dengue virus envelope protein after membrane fusion. *Nature* 427(6972):313-319.
35. Crispin M, *et al.* (2014) Uukuniemi phlebovirus assembly and secretion leave a functional imprint on the virion glycome. *J. Virol.* 88(17):10244-10251.
36. Kuismanen E (1984) Posttranslational processing of Uukuniemi virus glycoproteins G1 and G2. *J. Virol.* 51(3):806-812.
37. Pesonen M, Kuismanen E, & Pettersson RF (1982) Monosaccharide sequence of protein-bound glycans of Uukuniemi virus. *J. Virol.* 41(2):390-400.
38. Mueller DS, *et al.* (2008) Histidine protonation and the activation of viral fusion proteins. *Biochemical Society transactions* 36(Pt 1):43-45.
39. Kampmann T, Mueller DS, Mark AE, Young PR, & Kobe B (2006) The Role of histidine residues in low-pH-mediated viral membrane fusion. *Structure* 14(10):1481-1487.
40. Lozach P-Y, *et al.* (2010) Entry of bunyaviruses into mammalian cells. *Cell host & microbe* 7:488-499.
41. Qin ZL, Zheng Y, & Kielian M (2009) Role of conserved histidine residues in the low-pH dependence of the Semliki Forest virus fusion protein. *Journal of virology* 83(9):4670-4677.
42. Nayak V, *et al.* (2009) Crystal structure of dengue virus type 1 envelope protein in the postfusion conformation and its implications for membrane fusion. *Journal of virology* 83:4338-4344.
43. Fritz R, Stiasny K, & Heinz FX (2008) Identification of specific histidines as pH sensors in flavivirus membrane fusion. *The Journal of cell biology* 183(2):353-361.
44. Klimstra WB, Nangle EM, Smith MS, Yurochko AD, & Ryman KD (2003) DC-SIGN and L-SIGN can act as attachment receptors for alphaviruses and distinguish between mosquito cell- and mammalian cell-derived viruses. *Journal of virology* 77(22):12022-12032.
45. Tassaneetrithep B, *et al.* (2003) DC-SIGN (CD209) mediates dengue virus infection of human dendritic cells. *J Exp Med* 197(7):823-829.
46. Crispin M, *et al.* (2014) Structural plasticity of the Semliki Forest virus glycome upon interspecies transmission. *J Proteome Res* 13(3):1702-1712.
47. Hacker K, White L, & de Silva AM (2009) N-linked glycans on dengue viruses grown in mammalian and insect cells. *The Journal of general virology* 90(Pt 9):2097-2106.
48. Abrescia NG, Bamford DH, Grimes JM, & Stuart DI (2012) Structure unifies the viral universe. *Annual review of biochemistry* 81:795-822.
49. Aricescu AR, Lu W, & Jones EY (2006) A time- and cost-efficient system for high-level protein production in mammalian cells. *Acta Cryst. D* 62:1243-1250.
50. Walter TS, *et al.* (2005) A procedure for setting up high-throughput nanolitre crystallization experiments. Crystallization workflow for initial screening, automated storage, imaging and optimization. *Acta crystallographica. Section D, Biological crystallography* 61(Pt 6):651-657.
51. Gulick AM, Horswill AR, Thoden JB, Escalante-Semerena JC, & Rayment I (2002) Pentaerythritol propoxylate: a new crystallization agent and cryoprotectant induces crystal growth of 2-methylcitrate dehydratase. *Acta crystallographica. Section D, Biological crystallography* 58(Pt 2):306-309.
52. Winter G (2010) xia2: an expert system for macromolecular crystallography data reduction. *Journal of Applied Crystallography* 43(1):186-190.
53. Vonrhein C, Blanc E, Roversi P, & Bricogne G (2007) Automated structure solution with autoSHARP. *Methods in molecular biology (Clifton, N.J.)* 364:215-230.
54. Cowtan K (2006) The Buccaneer software for automated model building. 1. Tracing protein chains. *Acta crystallographica. Section D, Biological crystallography* 62(Pt 9):1002-1011.
55. Vagin AA, *et al.* (2004) REFMAC5 dictionary: organization of prior chemical knowledge and guidelines for its use. *Acta crystallographica. Section D, Biological crystallography* 60(Pt 12 Pt 1):2184-2195.
56. Adams PD, *et al.* (2010) PHENIX: a comprehensive Python-based system for macromolecular structure solution. *Acta Crystallographica Section D* 66(2):213-221.
57. Emsley P, Lohkamp B, Scott WG, & Cowtan K (2010) Features and development of Coot. *Acta crystallographica. Section D, Biological crystallography* 66(Pt 4):486-501.
58. Chen VB, *et al.* (2010) MolProbity: all-atom structure validation for macromolecular crystallography. *Acta crystallographica. Section D, Biological crystallography* 66(Pt 1):12-21.
59. Brennan B, *et al.* (2015) Reverse genetics system for severe fever with thrombocytopenia syndrome virus. *Journal of virology* 89(6):3026-3037.
60. Larkin, M.A. et al. Clustal W and Clustal X version 2.0. *Bioinformatics* **23**, 2947-8 (2007).
61. Heckman, K.L. & Pease, L.R. Gene splicing and mutagenesis by PCR-driven overlap extension. *Nature protocols* **2**, 924-32 (2007).
62. Swei, A. et al. The genome sequence of Lone Star virus, a highly divergent bunyavirus found in the Amblyomma americanum tick. *PLoS One* **8**, e62083 (2013).
63. Sievers, F. et al. Fast, scalable generation of high-quality protein multiple sequence alignments using Clustal Omega. *Molecular systems biology* **7**, 539 (2011).
64. Robert, X. & Gouet, P. Deciphering key features in protein structures with the new ENDscript server. *Nucleic Acids Res* **42**, W320-4 (2014).
65. Neville, D.C., Dwek, R.A. & Butters, T.D. Development of a single column method for the separation of lipid- and protein-derived oligosaccharides. *J Proteome Res* **8**, 681-7 (2009).
66. Pritchard, L.K. et al. Structural Constraints Determine the Glycosylation of HIV-1 Envelope Trimers. *Cell Rep* **11**, 1604-13 (2015).